Neuropsychology Review, Vol. 6, No. 2, 1996

Bilateral Comparison of Occipital Lobe Sulci: A Sulcus Identifying Algorithm

Z. Naor,[1] Y. Yeshurun,[1] and M. Myslobodsky[2,3]

A procedure for automatic identification of sulci of cerebral hemispheres in magnetic resonance images is presented. The algorithm departs from information of the spatial location of a given feature (e.g., sulcal contour) in one hemisphere and automatically defines its course in the other hemisphere. The automatic tracing of sulci was successfully performed in the mesial aspect of both hemispheres in 18 normal individuals. The sulcal location in the target hemisphere was first approximated by assuming an affine transformation between hemispheres, and then refined by local edge analysis. The method produced reliable results in comparing the intersulcal areas (the cuneus), sulcal length, their complexity, and the angle between the pariteooccipital and retrocalcarine fissures.

KEY WORDS: magnetic resonance imaging; image analysis; computerized data processing; occipital lobe; hemisphere asymmetries.

INTRODUCTION

The image formation based on the principle of nuclear magnetic resonance lead to an entirely new methodology, magnetic resonance (MR) imaging (Lauterbur, 1973) that proved to generate brain pictures of unusual clarity. The MR images could be analyzed and quantified with the accuracy superior to that afforded by x-ray computed tomography (CT). The MR-based image quantification (morphometry) took several major directions. One chiefly updates the data banks accumulated with CT techniques, re-

[1]Department of Computer Sciences, Tel-Aviv University, Tel-Aviv 69978, Israel.
[2]Psychobiology Research Unit, Department of Psychology, Tel-Aviv University, Ramat Aviv 69978, Israel.
[3]To whom correspondence should be addressed.

rding areas and volumes of the ventricular system and fluid filled struc-es of clinical interest and the magnitude of hemisphere asymmetries ratta *et al.*, 1989). The other attempts to provide an accurate definition difficult (within the context of the CT methodology) areas, such as the ainstem, temporal lobes, and posterior fossa (Gaffney *et al.*, 1988; Sud-th *et al.*, 1989; Jack *et al.*, 1989). Still another focuses on the estimates size of separate brain structures and/or nuclei (Uematsu and Kaiya, 1988; k *et al.*, 1989; Filipek *et al.*, 1989; Casanova *et al.*, 1990). Regrettably, systematic analysis of the brain gyral and sulcal patterns that are visu-zed in MR images and the analysis of variance of their interhemisphere ofiles are still unduly neglected. Only few studies attempted an isolation the characteristic shapes of several major sulci (Steinmetz *et al.*, 1989; Myslobodsky *et al.*, 1990; Ebeling *et al.*, 1989). Consequently, the depend-le systems for unassisted identification and quantification of the topo-aphical arrangement of the complexity of brain folding are still lacking Weis and Haug, 1990).

The present study describes a technique that affords a reliable isolation several sulci on the mesial brain surface along with examples that con-m its utility for the quantification of individual differences in sulcal pat-ns. The algorithm for sulcus identification (ASI) operates as follows: the erator enters the spatial location of a given sulcus in one hemisphere, en ASI automatically finds a similar sulcus in the other hemisphere of same individual.

METHOD

The study is based on MR images of 20 volunteers (17–66 years of e) with homolateral ocular dominance and normal neurological history. l of them were right-handed subjects with the exception of one left-nded.

MR imaging was performed on a 0.5 Tesla Elscint (GYREX 5000 with atrix size of 256 × 256 as described elsewhere (Myslobodsky *et al.*, 1991). ne position of the head was adjusted under the control of repeated, mul-planar, fast-locating MR scans to align the interhemispheric fissure with e sagittal imaging plane. The whole brain was then evaluated using con-guous sagittal, coronal, and axial slices of 5 mm thickness. To obtain an lequate anatomical display, T1-weighted spin-echo sequences were applied R/TE = 470–600/14–40 msec). All scans were evaluated for ventricular e and configuration, hemisphere width, prominence of cortical sulci, the gree of skull deformity and signal asymmetries, etc. All images were read normal. Two scans were rejected due to inferior image qualities.

The ASI

The problem we face is the following: given two corresponding (CT or MR) images of the two human brain hemispheres, the algorithm must accept as input the spatial location of a given feature (i.e., sulcus) in one image, and automatically detect this feature in the image of the other hemisphere. This task is feasibly only if certain assumptions are made regarding the spatial relations between features in the two hemispheres, since if there is no continuous mapping between the two images, it is hard to imagine any algorithmic solution. The basic assumption we make in this work is that there exists an affine transformation that maps one hemisphere into the other. While evolutionary and developmental considerations might play a major role in the specification of the exact spatial relation between the hemispheres, we maintain that for our purposes, affine transformation, namely, a combination of shift, rotation, scaling and shear is an acceptable approximation of interhemispheral feature mapping in brain images.

The method was implemented on MR images of normal human subjects. The anatomical structures analyzed may best be appreciated by reference to Fig. 1. The later shows that the first step requires an identification on the parasagittal cut of the brain of three corresponding noncolinear points that represent easily recognizable cranial and intracerebral landmarks in one MR image. These points are sufficient for a complete description of the affine transformation. They reference sulci of interest with regard to the nasion–inion line (ni; anterior–posterior dimension) and the perpendicular reference from that line at the point of confluence of the retrocalcarine (rc) and the parieto-occipital sulci (PO; Fig. 1A).

The following step requires a selection of the region of interest (ROI). In the present study, ROI was a rectangle surrounding the confluence of the parieto-occipital and the retrocalcarine sulci (Fig. 1A). At this stage the computation is directed at a search of the corresponding point in the other, "target" hemisphere. This is conducted in two steps. First, the affine transformation is accomplished to compute a rough approximation of the area of interest in the target hemisphere (Fig. 1B). Then, local edge features between the two hemispheres are compared using cross correlation for a better precision in pinpointing the location of the targeted sulcus. The distance between the rough estimate (based on affine transformation) and the more accurate estimate is noted as a measure of anatomical local interhemisphere asymmetry. Finally, the skeletons of the corresponding sulci in the two hemispheres are automatically traced (Fig. 1B).

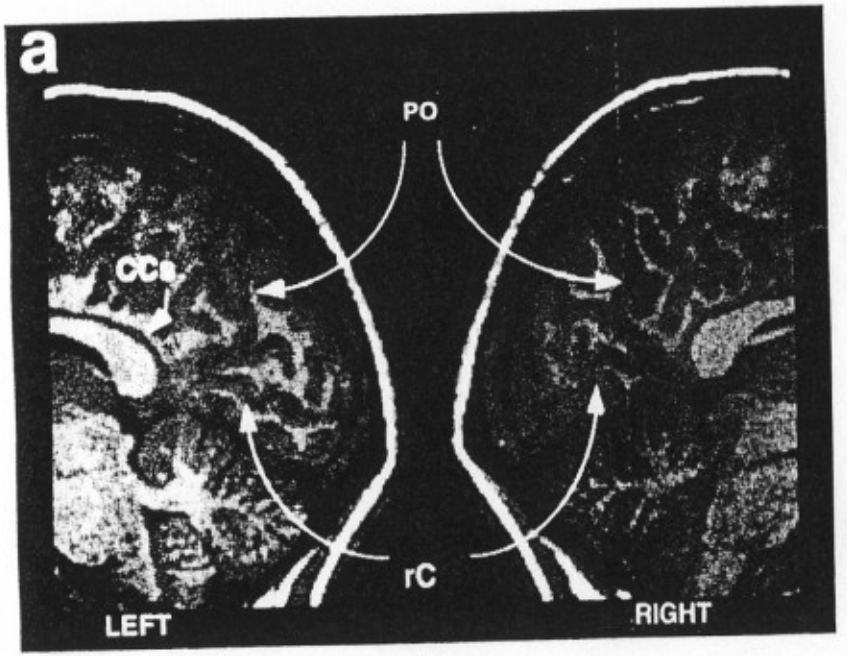

1A

Fig. 1. (a) MR images illustrate the anatomy of the caudal portion of the mesial surface of the right and left hemispheres. CCs: corpus callosum, splenium; PO parieto-occipital sulcus; rC: retrocalcarine sulcus. (b) Three reference points define invariant coordinate system in the right hemisphere. The confluence of the parieto-occipital (PO) and calcarine (C) sulci (PO-C point) is denoted by the cursor in the square. The ROI in the left hemisphere (depicted by the square) is found by the affine transformation computed from the right hemisphere parameters. The PO-rC location within the ROI is found by cross-correlation. After the PO-rC point is located, the sulcus skeleton (marked) is automatically traced and plotted along with their linear regression approximation (bottom left).

Tracing Algorithm

The tracing algorithm is based on a skeleton extraction routine. Skeletons are known to provide an accurate structural description of a shape, and several methods have been proposed and implemented for generation of skeletons from boundaries, such as medial-axis transformation (Blum, 1973; Shapiro, 1981). Their utilities recognized in reducing storage requirements, preserving topological properties of an image, and simplifying the computational procedures required for description and taxonomy. In the present study, the sulcal was defined as a path with local minimum cross-section intensity value. This definition is based on the observation that a

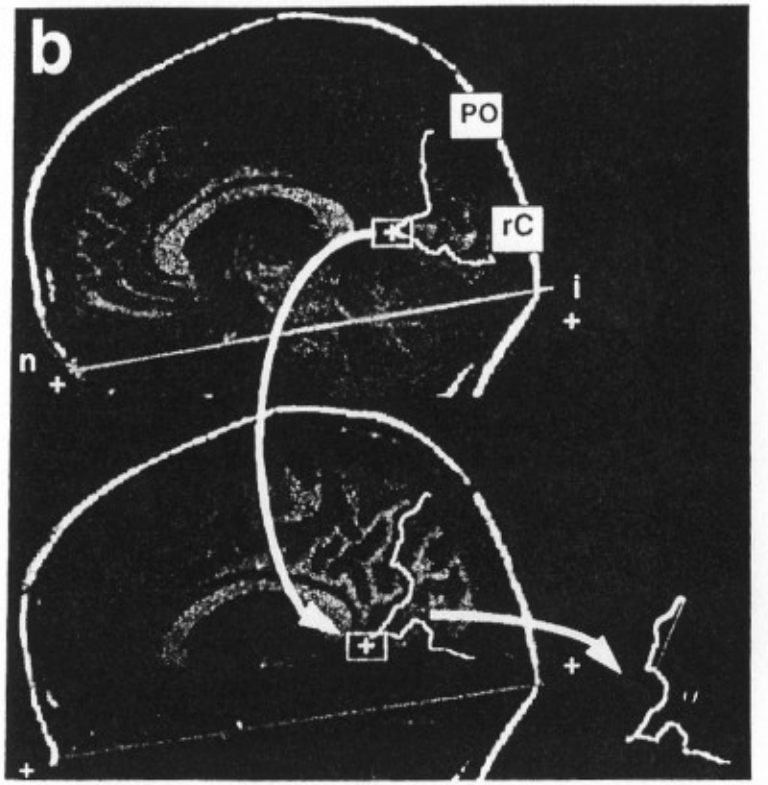

1B

typical intensity profile across a sulcus shows a local minimum at its center. In general, the sulcal gray level values are lower compared to those on its banks. Although this definition is relatively simple, in the sense that we do not seek for general definition to characterize all shapes by their skeleton, we found it to be satisfactory for our purposes. Taking into consideration that sulcal contours under study usually form a simple path (i.e., a path with no branching), our definition for sulcus line skeleton is in agreement with the usual definition. The ASI extracts the sulcus line skeleton in two steps. First, a particular point that belongs to the sulcus is selected, using local features of its surroundings, and its spatial location in the other hemisphere. Then, a tracing algorithm, which departs from that point, extracts the sulcus like skeleton. In the present study, that point was the confluence of the parieto–occipital and calcarine sulci (PO-C point).

The tracing starts with a preselected pixel, given as an input, which is used as a "seed" that belongs to a specific curve (e.g., the confluence of

the parieto–occipital and calcarine sulci). Then the fissure skeleton is grown with a serial detection process where each new element is suggested on the basis of already selected elements. To prevent tracing to proceed in reverse and to force tracing in a simple path, each skeleton pixel and its nearest eight neighbors are excluded from the next steps. The skeleton pixel is assigned the maximum intensity value. When the minimal weight of all eight primary directions accedes threshold value or when the tracing approaches the cranium, the algorithm terminates the search. The cranium is characterized as being signal void next to the local intensity maximum that can be detected by scanning the image from its peripheral aspect inward. The detection is further validated by identifying the outline of the brain. In a similar manner, the boundary of brain parenchyma adjacent to the skull is extracted and the tracing is terminated when the boundary is reached. We have also used dynamic programming to extract the sulcus, with similar results.

Image Analysis and Data Reduction

The following measures for the right and left hemispheres were taken. The length of the sulci (the parieto–occipital or retrocalcarine) was defined as the longest curve from the intersection between them and the border of the brain parenchyma. The triangular area between the parieto–occipital and retrocalcarine sulci was measured as the area of the cuneus. We have also assessed the complexity of the sulci by measuring the deviation of the sulcal skeleton from a straight line. This was carried out by calculating the area bounded between the skeleton and the linear regression line. In order to gain further insight into possible phenomena related to the sulci's complexity, we have calculated the Fourier Descriptors (Zahn and Roskies, 1972) of the sulcal skeletons. This measure estimates the spatial frequency of the curve, such that a winding curve has more high frequency Fourier Descriptors. There was no marked deviation between the results derived by using the two methods.

RESULTS

Figure 2 demonstrates individual traces derived from the right and left occipital lobe, which show good fit. To determine within-hemisphere variance for the whole sample, all individual traces of the calcarine and parieto–occipital sulci were superimposed separately for the right and left hemispheres. Figure 2 shows that sulcal traces on the right and left side scatter over practically identical areas, suggesting that interhemisphere

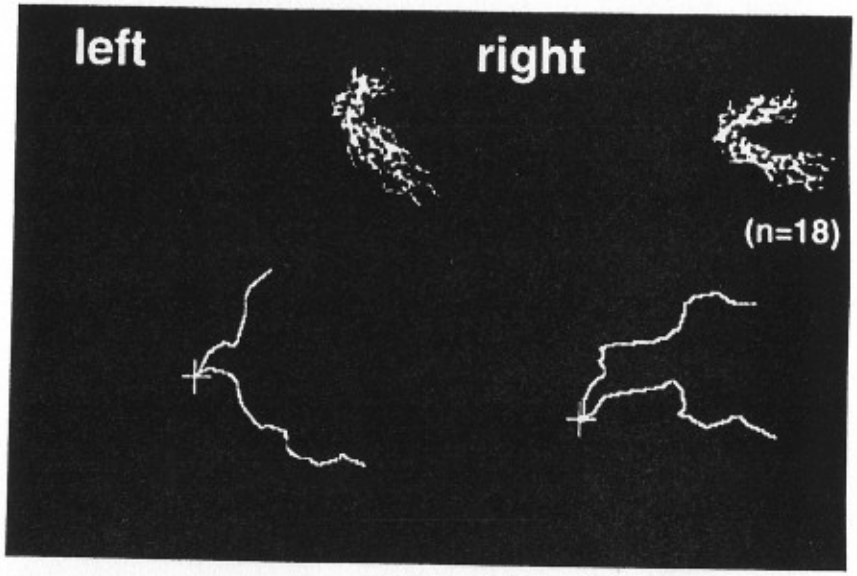

Fig. 2. Final result conducted on a set of noisy parasagittal brain images. Superposition of 18 sulcal traces for the right and left hemisphere.

asymmetry in the sampled region must be comparable. This impression was further examined by assessing several major sulcal measures obtained for the right and left hemispheres. These are the angle created by the parieto–occipital and calcarine sulci (PO-C angle), cuneal area, and sulcal complexity. Table I summarized the data along with the results of matched-pair *t* test. It shows a trend (albeit marginally significant) toward a more tortuous parieto–occipital sulcus in the left hemisphere. A similar trend of the left calcarine sulcus appeared to be nonsignificant. Table II demonstrates a significant degree of correlation between PO-C angle and cuneal area in the right and left hemispheres. In contrast, there was a meager right–left correlation of sulcal complexity measures.

DISCUSSION

The present study showed that ASI is a practical method that requires very limited training for the identification and quantification of sulci with a degree of accuracy of a skilled operator. Also, once a sulcus was traced, ASI automatically initiated a search of a similar pattern in windows or files (e.g., relevant sections of the same area of another hemisphere) as soon

Table I. Group Values of Sulcal Measures in the Right and Left Hemispheres ($X \pm SD$)[a]

Variable	Right	Left	$t(17)$	p
PO-C angle	85.5 (18.0)	90.9 (13.1)	1.33	0.2021
Cuneus area	3.06 (0.99)	3.26 (0.92)	1.23	0.2370
PO complexity	2.01 (0.87)	2.43 (1.00)	1.75	0.0984
C complexity	4.77 (1.86)	4.98 (1.69)	1.39	0.1842
Cos(NASION)	0.94 (0.03)	0.95 (0.02)	4.27	0.0006
Cos(INION)	0.69 (0.10)	0.69 (0.10)	0.23	0.8241

[a]PO: parieto-occipital; C: calcarine; Cos(NASION): cosine of {PO-C, NASION, INION} angle; Cos(INION): cosine of {PO-C, INION, NASION} angle.

Table II. Pearson Correlation Matrix for Sulcal Measures[a]

Variable	1	2	3	4	5	6
PO-C angle	0.47[b]					
Cuneus area		0.74				
PO complexity			0.195			
C complexity				0.14		
Cos(NASION)					0.09[b]	
Cos(INION)						0.77[b]

[a]See Table I for abbreviations.
[b]$p < 0.05$, one tailed.

as a familiar set of landmarks was entered. It should be noted that the acceptance criteria of the algorithm are determined by the contrast of neighboring pixels. Therefore, the process of skeletonization may be sensitive to noise and signal dropout in the image (i.e., regions where boundaries cannot be defined). This is known to happen due to anatomical variation with a lack of continuity in the sulcus. Such interruptions are infrequent and are expected to occur in the distal portions of the sulcus (Ono *et al.*, 1990). However, in a few cases, where the sulcus was interrupted, the algorithm was capable of bridging the gap. In fact, there was no overt detection failure (loss of trace) even in a relatively degraded image. Only in one case with a somewhat idiosyncratic sulcal pattern did the algorithm forced a false identification of the calcarine sulcus. Consistent with Myslobodsky *et al.* (1991), this is most likely when its course is interrupted by side branches, especially if they are connected with the paracalcarine sulcus.

Another advantage of ASI mentioned above, compared to available packages, is in that it permitted an automatic search, extraction, and quantification of the same feature in a different hemisphere. We used ASI for a problem that has a wide range of applications, in interpreting the electrophysiology of the visual system (Myslobodsky *et al.*, 1991; Srebro, 1990), neurosurgery (Stensaas *et al.*, 1974), in a search of anatomical correlates of brain laterality (Habib *et al.*, 1984; Geschwind and Levitsky, 1986), in identifying interindividual variance of sulcal profiles, etc. So far, the bilateral comparison of sulcal patterns was conducted interactively for the major brain sulci, such as the Central and Sylvian fissures (Habib *et al.*, 1984; Geschwind and Levitsky, 1986; Steinmetz *et al.*, 1989). The sulcal pattern of the occipital lobe is known to have a significant degree of complexity and individual variability (Connolly, 1950; Stensaas *et al.*, 1974). The results of the present study showed, however, that the asymmetry in the sulcal pattern in the occipital lobe is meager. This is consistent with the previous findings based on an interactive identification of occipital sulci on MR images (Myslobodsky *et al.*, 1991). However, the present finding suggests that sulcal complexity might be an acceptable measure of right–left differences in sulcal patterns. The interhemisphere correlation of this measure was minimal. The parieto–occipital sulcus appeared to be more tortuous in the left hemisphere. This result might prove significant with an increase in the sample size. In view of the exploratory nature of the study the same applies to a small and nonsignificant trend toward increased size of the left cuneus that is counter to the recent anatomical findings by Ono *et al.* (1990). We mention it to caution that the anatomy of the mesial part of the occipital pole size is expected to vary due to the selection of the midline in MR imaging. MR images in the sagittal plane are aligned with the interhemispheric fissure. The interhemispheric fissure may be curved in more than 30% of the subjects due to occipital falx deviation (Myslobodsky and Weinberger, 1987). As a result, the medical surface of the occipital lobe may not be coplanar with the surface of MR imaging. A slight increase in the size of the hemisphere may occur when the cut traverses the occipital pole. Also, given that the falx is typically deviated to the right (Myslobodsky and Bar-Ziv, 1989; Myslobodsky and Weinberger, 1987), a part of the left occipital pole could actually be imaged with the right hemisphere. The same problem could conceivably complicate the identification of the most caudal portion of the calcarine sulcus since the latter seldom reaches the end of the occipital pole (Stensaas *et al.*, 1974). Still another possible hazard is that our major cranial reference, the ni line, traverses external anatomical landmarks of exceptional variability. Formally defined, the nasion is the intersection of the fronto-nasal suture and the median plane (Howells, 1973). Given that the nasion was defined in cuts placed 5 mm from the midline, only the general fronto–nasal curve was visualized. Its deepest point that was read as the nasal root could vary and show asymmetry in the two paramedial cuts. The opposite landmark, the inion, is often difficult to define inasmuch as in MR images it is seen as a signal void and it may

not be coplanar with the interhemispheric fissure (Myslobodsky and Bar-Ziv, 1989; Myslobodsky *et al.*, 1991). Therefore, the right and left ni lines may not be strictly parallel. Thus the accuracy of sulcal identification on the mesial brain surface can be greatly improved by using the thinner cuts located close to the midline.

In summary, the algorithm may be helpful in identifying sulcal profile in any "twin" structure whenever a familiar set of landmarks were entered. ASI was explored in a rather simple terrain of the flattened medial aspect of the hemispheres with both sulci having practically uninterrupted course. The choice of the area was a compromise sufficient for our main purpose of examining the method.

ACKNOWLEDGMENT

This research was supported in part by a grant from the Ford Foundation (10710321), administered via the Israel Foundations Trustees, to MSM.

REFERENCES

Blum, H. (1973). Biological shape and visual science. *Journal of Theoretical Biology* 38: 205-287.

Casanova, M., Sanders, R., and Goldberg, T. (1990). Morphometry of the corpus callosum immonozygotic twins discordant for schizophrenia: A magnetic resonance imaging study. *Journal of Neurology and Neurosurgery* 53: 416-421.

Connolly, J. (1950). *External morphology of the primate brain.* C. C. Thomas, Springfield, IL.

Ebeling, U., Steinmetz, H., and Huang, Y. (1989). Topography and identification of the inferior precentral sulcus in mr imaging. *American Journal of Neuroradiology* 10: 937-942.

Filipek, P., Kennedy, D., and Caviness, V. S., Jr. (1989). Magnetic resonance imaging-based brain morphometry: Development and application to normal subjects. *Annals of Neurology* 25: 61-67.

Gaffney, G., Kuperman, S., and Tsai, L. (1988). Morphological evidence for brainstem involvement in infantile autism. *Biological Psychiatry* 24: 578-586.

Geschwind, N., and Levitsky, W. (1986). Human brain: Left-right asymmetries in temporal speech region. *Science* 161: 186-197.

Habib, H., Renucci, R., Vanier, M., Corboz, J., and Salamon, A. (1984). Ct assessment of right-left asymmetries in the human cerebral cortex. *Journal of Computer Assisted Tomography* 8: 922-927.

Howells, W. (1973). *Cranial Variation in Men.* Harvard University Press, Cambridge, MA.

Jack, C., Twomey, C., and Zinsmeister, A. (1989). Anterior temporal lobes and hippocampal formations: Normative volumetric measurements from mr images in young adults. *Radiology* 172: 549-554.

Lauterbur, P. (1973). Image formation by induced local interactions: Examples employing nuclear magnetic resonance. *Nature* 242: 190-191.

Myslobodsky, M., and Bar-Ziv, J. (1989). Locations of occipital electrodes verified by computed tomography. *EEG Clinical Neurophysiology* 72: 362-366.

Myslobodsky, M., Coppola, R., and Weinberger, D. (1990). EEG laterality in the era of structural brain imaging. *Brain Topography* 3: 381-390.

Myslobodsky, M., Glicksohn, J., Coppola, R., and Weinberger, D. (1991). Occipital lobe morphology in normal individuals assessed by magnetic resonance imaging. *Vision Research* 31: 1677-1685.

Myslobodsky, M., and Weinberger, D. (1987). Reversed brain anatomical asymmetries in schizophrenia: A search for contributing variables. In Ottoson, D. (ed.), *Duality and Unity of the Brain*, Macmillan, London, pp. 367-381.

Ono, M., Kubic, S., and Abernathey, C. (1990). *Atlas of Cerebral Sulci*, Stuttgart, Thieme Verlag.

Shapiro, L. (1981). Skeleton generation from x,y boundary sequences. *Computer Graphics and Image Processing* 15: 136-153.

Srebro, R. (1990). Realistic modeling of vep topography. *Vision Research* 30: 1001-1009.

Steinmetz, H., Furst, G., and Meyer, B. (1989). Craniocerebral topography within the international 10-20 system. *Electroencephalography and Clinical Neurophysiology* 72: 499-506.

Stensaas, S., Eddington, D., and Dobelle, W. (1974). The topography and variability of the primary visual cortex in man. *Journal of Neurosurgery* 40: 747-755.

Stratta, P., Possi, A., and Galucci, M. (1989). Hemispheric asymmetries and schizophrenia: A preliminary magnetic resonance imaging study. *Biological Psychiatry* 25: 275-284.

Suddath, R., Casanova, M., and Goldberg, T. (1989). Temporal lobe pathology in schizophrenia: A quantitative magnetic resonance imaging study. *American Journal of Psychiatry* 146: 464-472.

Uematsu, M., and Kaiya, H. (1988). Cerebellar vermal size predicts drug response in schizophrenic patients: A magnetic resonance imaging (mri) study. *Progress of Neuro-Psychopharmacological and Biological Psychiatry* 12: 837-848.

Weis, S., and Haug, H. (1990). The morphological substrate of cerebral asymmetry: the problem of its measurement. *Archives of Neurology* 47: 379.

Zahn, C., and Roskies, R. (1972). Fourier descriptors for plane closed curves. *IEEE Transactions on Computers* C-21: 269-281.